journal

J. Am. Ceram. Soc., 92 [10] 2323–2330 (2009)
DOI: 10.1111/j.1551-2916.2009.03199.x

First-Principles Study of Elastic Constants and Interlayer Interactions of Complex Hydrated Oxides: Case Study of Tobermorite and Jennite

Rouzbeh Shahsavari,[‡] Markus J. Buehler,[‡] Roland J.-M. Pellenq,[§,‡] and Franz-Josef Ulm[†,‡]

[‡]Department of Civil and Environmental Engineering, Massachusetts Institute of Technology, Cambridge, Massachusetts 02139

[§]Centre Interdisciplinaire des Nanosciences de Marseille, CNRS-Marseille Université, 13288 Marseille, France

It is a common perception that layered materials are soft in the interlayer direction. Herein, we present results of first-principles calculations of the structure and elastic constants of a class for hydrated oxides, tobermorite, and jennite, which illustrate that this is not the case, if (1) the interlayer distance is such that coulombic interlayer interactions become comparable to the iono-covalent intralayer interactions and (2) the existence of interlayer ions and water molecules do not shield the coulombic interlayer interactions. In this case, the mechanically softest directions are two inclined regions that form a hinge mechanism. The investigated class of materials and results are relevant to chemically complex hydrated oxides such as layered calcium–silicate–hydrates (C–S–H), the binding phase of all concrete materials, and the principle source of their strength and stiffness. In addition, the first-principles results may serve as a benchmark for validating empirical force fields required for the analysis of complex calcio–silicate oxides.

I. Introduction

By mixing water and cement, a complex hydrated oxide called C–S–H (calcium–silicate–hydrate), precipitates as nanoscale clusters of particles. Here the cement chemistry notation is used for C = CaO, S = SiO_2, H = H_2O. C–S–H is a nonstoichiometric gelatious oxide and the hyphenated expression refers to different combination of C, S, and H. C–S–H is the primary binding product of cement hydration,[1] and it is considered to be the elementary building block for concrete strength and durability. But despite its ubiquitous presence and decades of intensive research, the atomic arrangement of C–S–H remains an enigma. The average Ca/Si ratio in C–S–H is 1.7,[2] with local values measured by transmission electron microscopy (TEM) between 0.6 and 2.3.[3] High-resolution ^{29}Si, ^{1}H, and ^{17}O nuclear magnetic resonance (NMR), X-ray adsorption spectroscopy, IR spectroscopy, and Raman spectroscopy revealed important information about C–S–H structures.[4] It is widely accepted that C–S–H has a layered structure akin mostly to that of tobermorite and jennite minerals. Because of their similar chemical composition and similar crystal structure, tobermorite and jennite minerals have been suggested as possible model crystals for the C–S–H structure.[3,5] The focus of this paper is twofold:

(1) To present first-principles calculations on the structure and mechanical properties of such a family of complex hydrated oxides, tobermorite polymorphs, and jennite. Among mechanical properties, the calculation of elastic constants is the first and most fundamental concern because many other properties such as phase-transition, mechanical stability, and fracture energy can be related to them. Such first-principles results may also serve as a benchmark for validation of empirical force fields commonly employed in atomistic simulations of complex hydrated oxides.[6]

(2) To analyze and unravel the nature of interlayer bonds in this class of chemically complex layered oxides. A common feature of many layered structures are strong inplane interatomic bonds with only very weak bonds between the layers; which suggests that the layer direction is the softest direction. By means of an investigation on the nature of interlayer interactions, we show that this class of hydrated oxides has a distinctive behavior away from the common intuition.

The paper is organized as follows: Basic structural components of the tobermorite family and jennite are reviewed in Section II. The computational method is presented in Section III. Section IV presents the results including lattice parameters, elastic constants, interlayer interaction mechanisms, and averaged mechanical properties. These results are discussed in Section V.

II. Mineral Analogs of C–S–H

Different models define the C–S–H gel as calcium oxide sheets connected to silicate chains to form a layered structure.[7–9] There are at least 30 crystalline minerals that are similar in composition to C–S–H. However, even though their overall chemical composition is similar, they differ in the atomic arrangement, the Ca/Si ratio and the number of OH and H_2O groups.[1] High-resolution TEM observations indicate that the C–S–H gel contains mostly tobermorite and jennite-like structures.[3,5] Very recently, the atomic structure of tobermorite polymorphs and jennite was reported,[10–13] from extensive X-ray diffraction Rietveld analyses.

(1) Tobermorite Minerals

Figures 1(a) and (b) show respectively a top view of tobermorite with silica chains connected to calcium ribbons, and a side view of tobermorite with two layers (the interlayer water molecules and interlayer calcium ions are not shown in this figure). The silica chains are connected to calcium layers from both top and bottom. These chains are Wollastonite type or Dreierketten in which the minimum length of the repeating unit contains three tetrahedra. Two of the tetrahedra share an oxygen in a dome-type pattern and are called paired tetrahedra while the third tetrahedron which points out of the calcium layer, is called bridging tetrahedron. NMR studies show that C–S–H has a structure very similar to this form.[7–9] Tobermorite groups are layered structures and can be classified based on their different basal spacing as 9.3×10^{-10}, 11.3×10^{-10}, and 14×10^{-10} m[14] which are usually referred to as 9, 11, and 14 Å tobermorite minerals.[10–12,14] This interlayer spacing distance represents the degree of hydration of tobermorite, a property that changes through heating.[15–20] The interlayer distance can in general

H. Jennings—contributing editor

Manuscript No. 25826. Received February 4, 2009; approved May 7, 2009.
Financial support by CIMPOR Corporation, Portugal, enabled through the MIT–Portugal program, is gratefully acknowledged.
[†]Author to whom correspondence should be addressed. e-mail: ulm@mit.edu

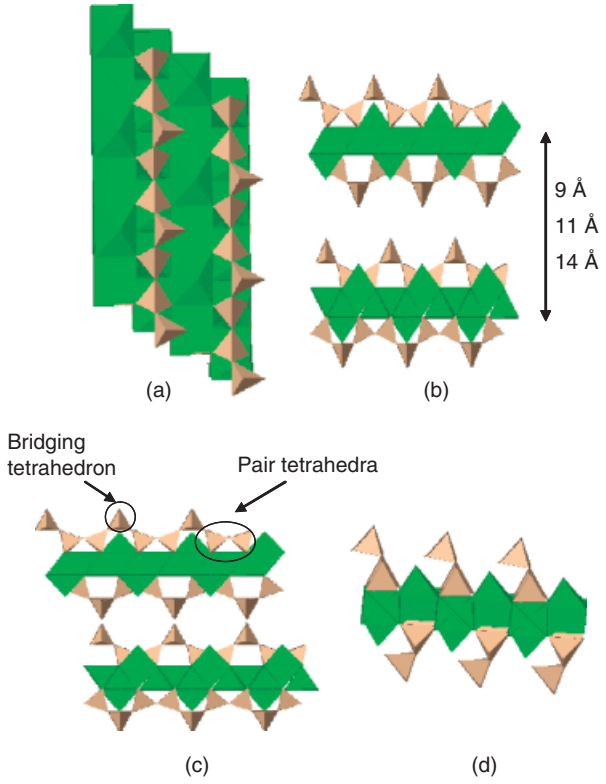

Fig. 1. (a) Top view of a typical tobermorite. Small pyramids represent silicon tetrahedra. (b) Side view of a layered tobermorite with single silica chains. (c) A side view of a layered tobermorite with double silica chains. (d) [010] view showing the dangling bridging tetrahedra.

contain water molecules and Ca cations (or other cations) depending on the hydration degree (water content) and chemical composition.

A head-to-head connection of bridging tetrahedra (such as in Fig. 1(c)) form a ring-type shape that is called double silica chain. Otherwise, it is called a single silica chain with dangling bridging tetrahedra in the interlayer distance (Fig. 1(b)). A [010] view of tobermorite and the flanking bridging tetrahedra is shown in Fig. 1(d). Two different structures for tobermorite 11 Å can be found: The Merlino structure with chemically bonded layers (double silica chain),[11] and the Hamid structure that depicts tobermorite as independent layers with single silica chains.[21] While the crystal size is unchanged experimentally, the Hamid's tobermorite structure can have three different Ca/Si ratios, namely 0.67, 0.83, and 1. Tobermorite 11 Å (Hamid and Merlino) and tobermorite 14 Å are monoclinic crystals while tobermorite 9 Å is a triclinic crystal.

(2) Jennite

Jennite is an another analogous C–S–H crystalline mineral that is believed to be closely related to the structure of C–S–H at late stages of the hydration process.[1] ^{29}Si NMR indicates that it has single silica chains[17] with Ca/Si = 1.5. Its triclinic crystal structure is solved and refined in Bonnacorsi *et al.*[13] Figure 2(a) shows a layer of jennite along with a unit cell. Figure 2(b) shows a side view of jennite.

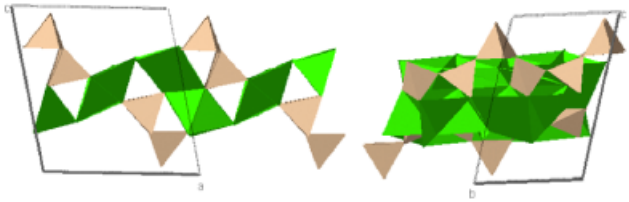

Fig. 2. (a) A layer of jennite along with is unit cell. *a*, *b*, and *c* are the unit cell vectors (b) [100] view of jennite.

III. Computational Methods

Akin to experimental approaches, the use of first-principles simulation techniques to identify core properties of materials requires some technical details about the simulation tools employed in this study. There are very limited number of first-principles study on the structure of tobermorite and jennite, [22,23] here we extend those approaches to the structure and elastic constants of these minerals. Except otherwise stated, all calculations reported in this paper are performed by Density Functional Theory (DFT)[24,25] using GGA exchange correlation functionals. For energy and stress calculations we used ultrasoft pseudopotentials[26] with a plane wave basis set and a cutoff energy of 420 eV for the wavefunctions and 50350 eV for the charge density, as implemented in the PWSCF package of Quantum Espresso distribution.[27]

Considering first-principles calculations, it is important to ensure that the convergence in *k*-point sampling and plane wave energy cutoffs are satisfactory. However, the computational costs grow exponentially when the system size becomes large, and thus there is a trade-off. In our study, as the system sizes were relatively large ($\approx$70 to $\approx$100 atoms per unit cell) we used γ-point-sampling of the Brillouin zone.

Before calculating the elastic properties, we perform 0 *K* energy minimizations as implemented in PWSCF to fully relax the crystals. The importance of obtaining the equilibrium state is first, to avoid any possible metastable state and second, to make sure that the current state is not far from the regions where linear elasticity holds. To achieve equilibrium ground state the following two criteria are met concurrently: each of the stress components is below 0.5 kbar; each of the *X*, *Y*, and *Z* component of the force on any single atom is below 0.01 eV/A.

Once all crystalline minerals have attained relaxed states, we apply strains to the cell coordinates to calculate elastic constants. We use stress–strain approach to calculate the elastic constants,[28] which allows one to obtain second-, third-, and fourth-order elastic constants. In this method, for each strain, by calculating the stress tensor, one can construct a linear system relating stresses to strains. Then using an orthogonal matrix factorization and the best least square fit, elastic constants are found. Further details of this technique and its application to a wide range of ceramics can be found in Yao *et al.*[29] and references cited therein. The generalized Hooke's law in linear elasticity is given by

$$\begin{bmatrix}\sigma_1\\ \sigma_2\\ \sigma_3\\ \sigma_4\\ \sigma_5\\ \sigma_6\end{bmatrix} = \begin{bmatrix} C_{11} & C_{12} & C_{13} & C_{14} & C_{15} & C_{16}\\ & C_{22} & C_{23} & C_{24} & C_{25} & C_{26}\\ & & C_{33} & C_{34} & C_{35} & C_{36}\\ & & & C_{44} & C_{45} & C_{46}\\ & & & & C_{55} & C_{56}\\ & & & & & C_{66}\end{bmatrix}\begin{bmatrix}e_1\\ e_2\\ e_3\\ e_4\\ e_5\\ e_6\end{bmatrix} \quad (1)$$

Because the crystalline minerals under investigation are either monoclinic or triclinic, we apply all six strains. By applying any nonzero strain in Eq. (1) and calculating stresses, one can determine a column of elastic constants. Thus by repeating this procedure for all strains we cover the whole elastic tensor. In this method, off-diagonal components appear twice in the calculations and to have a better estimate we take the average of the two equivalent off-diagonal terms.

As elastic constants are defined in an orthogonal coordinate system, we relate cell parameters to Cartesian system *XYZ* (subindex 1 in Eq. (1) refers to *X*-axis; 2 to *Y*-axis and 3 to *Z*-axis) in the following way: the first cell parameter, *a*, is parallel to *X*-axis; second cell parameter, *b* is in the *XY* plane and finally the third cell parameter, *c*, is a vector in *XYZ* space. The variables

e_4, e_5, and e_6 are the shear strains between YZ, XZ, and XY planes, respectively. We apply both positive (stretch) and negative (compression) strains. Thus in total we perform 12 simulations for each crystal. Next, using least square method, we minimize

$$\left|\left(\sigma_i - \sigma_i^r\right) - C_{ij}\left(e_i - e_i^r\right)\right| \quad (2)$$

where σ_i^y and e_i^y are residual stress and residual strain, respectively, and $(e_i - e_i^r)$ is the applied strain. In this way, the uncertainty in C_{ij} values will be minimized with enhanced overall accuracy. Choosing the correct magnitude for the applied strain is critical. Sufficiently small strains are needed to ensure that elastic constants are within the linear theory of elasticity, but this will require higher precision accuracy in calculating the total energy and forces on each atom. This is computationally very expensive, and therefore there is a trade-off between the desired level of accuracy and computational time. In practice it has been shown that 1% strain is sufficiently accurate for calculating elastic constants.[29,30] Thus we use ± 0.01 for all strains and let the system relax after each strain because electronic vibrations are coupled to ionic motions. Once we obtain the elastic constant tensor we invert it to obtain the compliance tensor by $S_{ij} = C_{ij}^{-1}$, where the first three diagonal terms of the compliance tensor, S_{11}, S_{22}, S_{33}, represent the inverse of Young's modulus in the corresponding X, Y, and Z directions, respectively.

In order to calculate the partial atomic charges, we performed variational static calculations at the Hartree–Fock (HF) approximation (without a posteriori account for electron correlation effects) using the CRYSTAL code developed for solid-state applications.[31] Multielectron wave functions are described by linear combination of crystalline orbitals expanded in terms of Gaussian-type basis sets. Considering the system size, we have chosen the 6-31G* split valence basis set for O[29] and the standard 6-21 G for H. Ca and Si species are implemented as described by Barthelat and Durand pseudo potentials, respectively.[31] Convergence parameters were set for a high level of accuracy (ITOL1 = ITOL2 = ITOL3 = 5, ITOL4 = 6, ITOL5 = 11). Atomic partial charges were determined following the Mulliken partitioning scheme. This provides an easy way to characterize the type of bonding schemes (covalent, iono-covalent, coulombic) that are in action.

DFT at its current state of development may not yield accurate van der Waals dispersion forces.[33,34] In C–S–H models, the interlayer interactions are dominated by coulombic forces rather than van der Waals dispersion forces.[6] Thus the predicted interlayer interactions for C–S–H models should not be affected by this issue. In this work, we used Jmol[35] to create 3D visualizations of the crystal structures.

IV. Computational Results

(1) Cell Parameters and Elastic Constants

Table I shows the cell parameters for the studied C–S–H models obtained by first-principles calculations. Compared with experiments, the average error of these results is typically $<1\%$, and the maximum error is approximately 3% for tobermorite 11 Å (Hamid) Ca/Si = 0.67. This error may stem partly from 0 K temperature conditions used in first-principles calculations versus room temperature in experiments, and may also be due to the fact that the final stress components during the course of relaxation are not exactly zero. Thus it is expected that there could be small residual stresses that disturb the equilibrium lattice parameters.

Table II summarizes the elastic constants obtained from first-principles calculations. Tobermorite 9 Å and jennite (triclinic crystals) have 21 independent second-order elastic constants. The remaining crystals which are monoclinic have only 13 independent elastic constants.[36] For monoclinic crystals we assumed that the unique axis is in the direction of the c cell parameter.

For tobermorite 9 Å we were able to compare the results with higher k-points sampling (four k-points with a mesh of $2 \times 2 \times 1$ using Monkhorst-Pack scheme.[37] In this case, the maximum errors on lattice parameters and elastic constants were $<0.3\%$ and 2 GPa, respectively. The use of GGA exchange correlation potentials lead to larger exchange correlation energy and therefore favor longer bonds. This results in lattice parameters that are overall larger than experiments, and elastic constants that are slightly underestimated.

(2) Hinge Deformation Mechanism in Tobermorite 9 and 11 Å

In this section, via classical rotation of the compliance tensors[36] we focus on Young's modulus along any arbitrary direction. This enables us to identify the critical directions of a crystal where the softest or stiffest Young's moduli are located. While we performed this analysis for all crystals, here we only report the findings for tobermorite 11 Å.

Table I. First-Principles Calculation of Cell Parameters for the Tobermorite Family and Jennite

	Cell parameter	a (Å)	b (Å)	c (Å)	α (deg.)	β (deg.)	γ (deg.)
Tobermorite 14 Å	Experiment	6.735	7.425	27.987	90	90	123.25
$Ca_5Si_6O_{16}(OH)_2 \cdot 7H_2O$	*Ab initio*	6.87	7.43	28.49	89.96	90.05	123.47
Ca/Si = 0.83	Error (%)	2.00	0.13	1.80	0.006	0.004	1.31
Tobermorite 11 Å (Merlino)	Experiment	6.735	7.385	22.487	90	90	123.25
$Ca_4Si_6O_{15}(OH)_2 \cdot 5H_2O$	*Ab initio*	6.80	7.51	22.572	89.83	89.05	123.43
Ca/Si = 0.67	Error(%)	1.00	1.70	0.38	0.18	1.00	0.15
Tobermorite 9 Å	Experiment	11.156	7.303	9.566	101.08	92.83	89.98
$Ca_5Si_6O_{16}(OH)_2$	*Ab initio*	11.211	7.389	9.710	102.65	92.54	89.75
Ca/Si = 0.83	Error (%)	0.49	1.17	1.5	1.55	0.28	0.25
Tobermorite 11 Å (Hamid)	Experiment	6.69	7.39	22.779	90	90	123.49
$Ca_6Si_6O_{18} \cdot 2H_2O$	*Ab initio*	6.60	7.40	23.13	90.00	90.00	123.62
Ca/Si = 1	Error(%)	1.4	0.08	1.5	0	0	0.11
Tobermorite 11 Å (Hamid)	Experiment	6.69	7.39	22.779	90	90	123.49
$Ca_5Si_6O_{16}(OH)_2 \cdot 2H_2O$	*Ab inito*	6.708	7.373	22.54	90	90	123.71
Ca/Si = 0.83	Error (%)	0.27	0.22	1.00	0	0	0.18
Tobermorite 11 Å (Hamid)	Experiment	6.69	7.39	22.779	90	90	123.49
$Ca_4Si_6O_{14}(OH)_4 \cdot 2H_2O$	*Ab inito*	6.898	7.371	22.153	90	90	124.64
Ca/Si = 0.67	Error (%)	3.10	0.24	2.74	0	0	0.9
Jennite	Experiment	10.575	7.265	10.931	101.3	96.98	109.65
$Ca_9Si_6O_{18}(OH)_6 \cdot 8H_2O$	*Ab inito*	10.702	7.342	10.891	102.11	95	109.82
Ca/Si = 1.5	Error (%)	1.2	1.06	0.36	0.8	2.0	0.16

Table II. First-Principles Calculation of Elastic Constants for the Tobermorite Family and Jennite

	Tobermorite (Merlino)			Tobermorite (Hamid, 11 Å)			Jennite
Elastic constant (GPa)	14 Å	11 Å	9 Å	Ca/Si = 1	Ca/Si = 0.83	Ca/Si = 0.67	Ca/Si = 1.5
C_{11}	77.60	116.95	169.15	148.25	131.95	102.65	100.1
C_{12}	35.90	45.83	54.48	63.25	48.30	41.68	26.85
C_{13}	20.18	27.88	37.45	26.75	23.15	27.70	32.03
C_{14}	0	0	−1.05	0	0	0	1.30
C_{15}	0	0	−8.90	0	0	0	1.45
C_{16}	3.08	0.3	2.7	6.63	−6.55	1.25	3.30
C_{22}	104.5	126.10	169.95	138.35	128.30	125.05	45.70
C_{23}	26.3	46.20	36.15	32.55	30.63	18.83	4.40
C_{24}	0	0	3.55	0	0	0	7.35
C_{25}	0	0	−11.75	0	0	0	−6.20
C_{26}	−1.75	−14.93	−1.08	1.85	−10.98	−4.10	−3.18
C_{33}	32.05	126.35	92.70	68.40	83.85	83.80	59.15
C_{34}	0	0	2.60	0	0	0	−1.30
C_{35}	0	0	−3.45	0	0	0	1.40
C_{36}	3.03	−9.35	0.60	−1.73	−8.58	−3.38	0.07
C_{44}	24.5	30.20	40.60	32.75	26.00	22.90	21.95
C_{45}	−9.43	−11.10	0.43	−1.93	−8.35	−11.93	−1.73
C_{46}	0	0	−5.48	0	0	0	−1.6
C_{55}	14.65	20.75	17.85	25.65	21.75	23.25	21.00
C_{56}	0	0	−1.85	0	0	0	2.73
C_{66}	38.10	44.35	45.65	53.30	49.35	50.20	26.55

Because tobermorite minerals have layered structures, it is expected intuitively that the softest direction is perpendicular to the layers and hence parallel to the interlayer direction. This is the case for tobermorite 14 Å with the interlayer stiffness $C_{33} = 32$ GPa, which is about 18% of the average intralayer stiffness. However, when the interlayer distance is decreased to 11 Å or less, in contrast to this conjecture, we find that the interlayer direction is not always the softest direction. For tobermorite 11 Å there are two possible structural forms:

Case 1. Hamid Structure: In Hamid structures, it is hypothesized that the layers are not connected through covalent bounds, instead the layers interact via long range coulombic forces.[38] To validate this hypothesis, we calculate the atomic charges at different interlayer distances. Table III shows that the average partial charges for tobermorite Ca/Si = 0.83 at the interlayer distance of 11 and 14 Å remain unchanged (except for a small redistribution of partial charges in water molecules due to the different adsorption sites). Thus pulling the layers apart does not involve any covalent bond breakage. Otherwise, the partial atomic charges should have been changed upon stretching and bond breakage. Hence, there exists no covalent bonds in between the layers; instead long-range coulombic forces form the interlayer interactions. As an example, Fig. 3(a) shows a unit cell of tobermorite 11 Å (Hamid) with Ca/Si = 0.83. In Fig. 3(b) the sphere with the unit radius represents directional Young's modulus for this structure. In view of Fig. 3(b), it turns out that the interlayer directions is not the softest direction and there are two inclined soft regions (blue area on the sphere). Considering Table II, in tobermorite 11 Å (Hamid) with Ca/Si = 0.83, the coulombic interlayer interactions—which results in $C_{33} \approx 85$ GPa – are now comparable to the iono-covalent intralayer interactions (C_{11}, $C_{22} \approx 130$ GPa). However, this requirement does not necessarily make two inclined soft regions in layered structures. Figure 4 shows the top views for different isomorphs of tobermorites 11 Å (Hamid type) with Ca/Si = 0.67, 0.83, and 1. These three isomorphs of Hamid structures are formed by adding (removing) an interlayer Ca and removing (adding) two protons. It is interesting to note that by increasing Ca/Si ratio, the two inclined soft regions (blue regions) shift toward the interlayer direction. Therefore at Ca/Si = 1, the interlayer direction becomes the softest direction.

Table III. Partial Charges for Tobermorite (Hamid Structure) Ca/Si = 0.83 at the Interlayer Distance of 11 and 14 Å

Partial charges	Si_{intra}	Ca_{intra}	Ca_{inter}	O_{intra}	O_w	H_w
Interlayer distance 11 Å	+2.24	+1.66	+1.72	−1.2	−0.88	+0.44
Interlayer distance 14 Å	+2.24	+1.66	+1.72	−1.2	−0.8	+0.4

The subindices " inter," "intra," and "W" refer to interlayer, intralayer, and water, respectively.

In order to investigate this later effect further, we quantify the total coulombic energy in the interlayer direction for each isomorph. To do so, we identically increase the interlayer distance for each Ca/Si ratio and relax the structure using DFT method. This allows us to monitor the change in total coulombic energy for each case. For a 0.3 Å interlayer displacement, the change in Ewald corrected coulombic energy for Ca/Si = 0.67, 0.83, and 1 is, respectively, $1.08\frac{eV}{Å^3}$, $0.78\frac{eV}{Å^3}$, and $0.46\frac{eV}{Å^3}$ per unit cell. This indicates that adding extra Ca ions (increasing Ca/Si ratio) in the interlayer distance reduces the contribution of coulombic interlayer interactions and hence shields the long-range interlayer bonds. This eventually leads to shifting the two inclined soft regions to a single straight interlayer direction (Fig. 4).

Case 2. Merlino Structure: Figure 5(a) shows a side view of the tobermorite 11 Å (Merlino) unit cell. The arrows indicate the direction of the softest Young's modulus. Figure 5(b) gives a top view of the same unit cell indicating two equivalent soft regions (blue color). In this case, the interlayer direction is considerably strengthened by covalent Si–O–Si interlayer bounds, which is due to the presence of double silica chains (head-to-head connection of bridging tetrahedra). From a structural point of view it thus appears as if the unit cell is easier to pull (or push) along the blue regions. Therefore, the shared oxygen atom of the double silica chain acts as a hinge, and the entire set of upper and lower atoms can pivot around this point. This is illustrated in Fig. 5(a) by blue and black arrows. Similar to tobermorite 11 Å (Merlino), there are covalent interlayer bonds in tobermorite 9 Å, which lead to the hinge mechanism. Physically the hinge mechanism implies that atomic reorientations are preferred over straight bond stretches to achieve the minimum energy. Because of the covalent interlayer bonds, the strengthening of the inter-

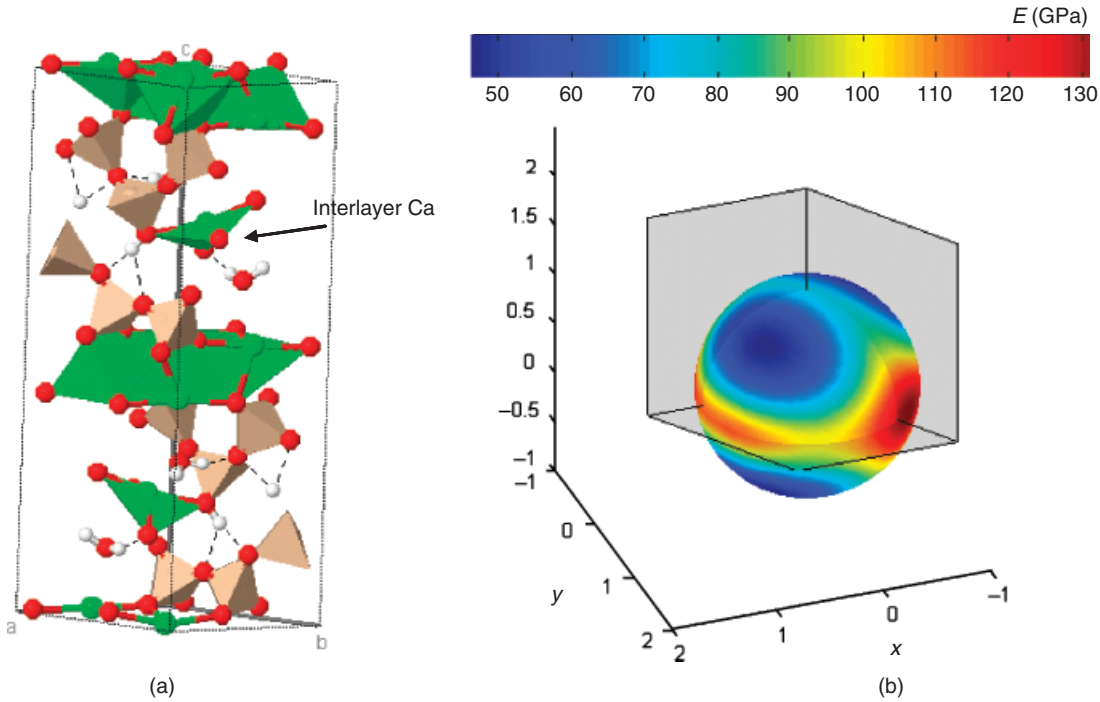

Fig. 3. Tobermorite 11 Å (Hamid) Ca/Si = 0.83. (a) Fully relaxed unit cell. Pink pyramids are silicon tetrahedra; green ribbons are calcium polyhedra; red circles are oxygen atoms and white circles are hydrogen atoms. (b) Young's modulus in any arbitrary direction. Any point on the sphere with the unit radius represents the tip of a unit vector, which is drawn from the center of the sphere (intersection of the three crystal planes). The surface of the sphere covers all possible 3D arbitrary unit vectors.

layer interactions in Merlino structure is less surprising than those in Hamid structures; and perhaps inconsistent with the common perception.

There are, indeed, hinge deformation mechanisms in tobermorite (Hamid) with Ca/Si = 0.67 and 0.83 (but not for Ca/Si = 1). However, unlike tobermorite 11 Å (Merlino), because there are no interlayer covalent bonds in Hamid structures, no particular atom acts as a hinge point. Instead a chemical site in the interlayer space becomes the center for such mechanism.

(3) Averaged Elastic Properties

To compare with measurements of elastic properties of C–S–H gels, it is useful to characterize the single-crystal level elastic properties. We use the Reuss–Voigt–Hill approximation[39–41] to calculate the bulk modulus, K, shear modulus, G, and average Young's modulus, E. One can also relate K and G to the plane-stress modulus M, which is accessible for example by indentation techniques based on the Hertz theory contact solution.[42,43] In the isotropic case, M relates to the bulk and shear modulus (K, G) of the indented half-space by

$$M = 4G\frac{3K+G}{3K+4G} \tag{3}$$

Table IV provides the values of the average elastic properties for tobermorite and jennite. Accurate nanoindentation experiments performed on C–S–H, indicates $M \approx 65$ GPa for solid C–S–H phases (Table III in Constantinides and Ulm,[44] Table II in Ulm *et al.*[45]). They are somewhat close to M values of tobermorite 14 Å and jennite ($M \approx 56$ GPa). This confirms earlier hypotheses[7,46] that tobermorite 14 Å and jennite are among the best C–S–H analogs. It is interesting to note that tobermorite 14 Å and jennite have almost the same values for all average elastic properties. This is of some importance, because it has been

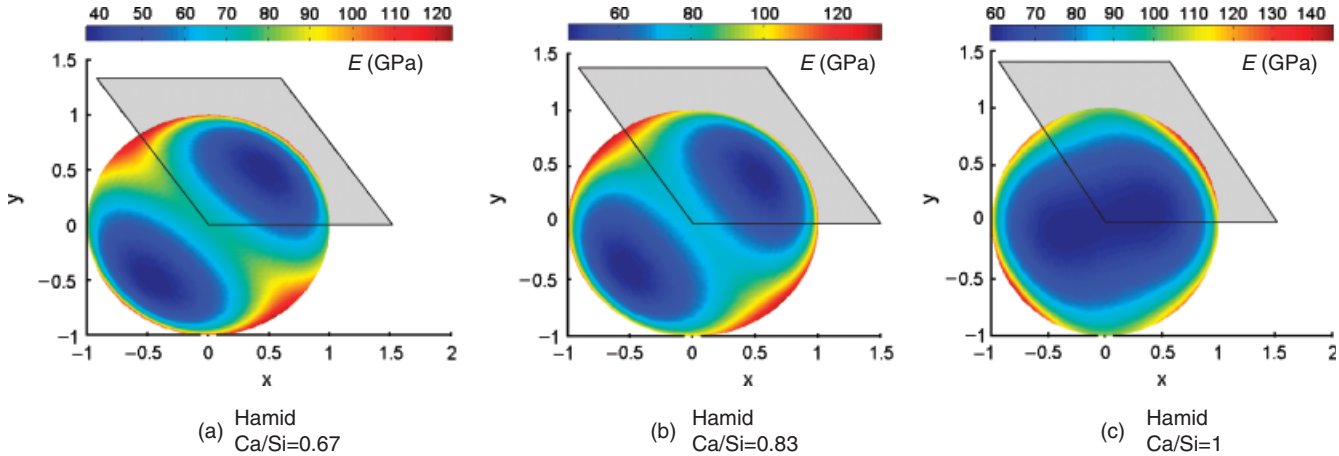

Fig. 4. Top views for tobermorite 11 Å (Hamid). (a) Tobermorite 11 Å (Hamid) Ca/Si = 0.67, (b) tobermorite 11 Å (Hamid) Ca/Si = 0.83, (c) tobermorite 11 Å (Hamid) Ca/Si = 1. Any point on the spheres with the unit radius represents the tip of a unit vector, which is drawn from the center of the spheres (intersection of the three crystal planes). In this figures, two of the crystal planes are perpendicular and are not seen. The surface of the spheres cover all possible 3D arbitrary unit vectors.

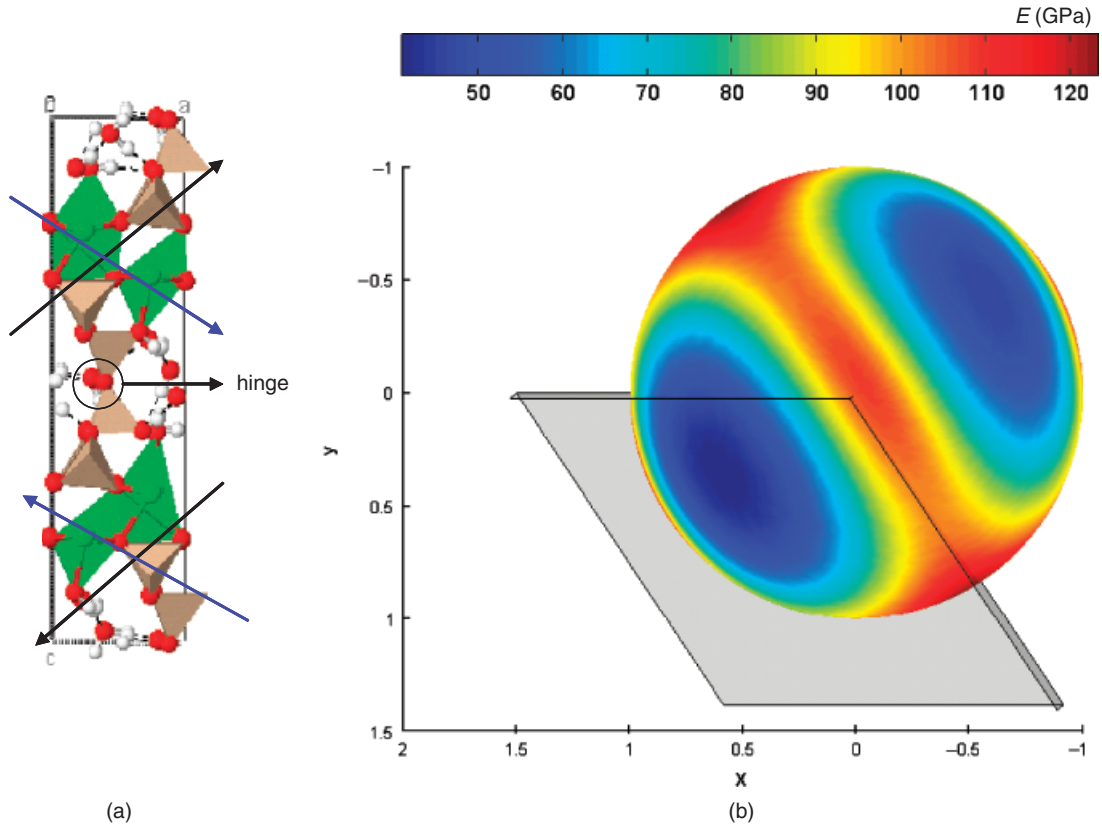

Fig. 5. Tobermorite 11 Å (Merlino): (a) side view of : blue (or black) coupled arrows indicate the deformation mechanism along the softest Young's modulus. (b) A top view of directional Young's modulus representing two equivalent inclined soft regions. The embedded lines on the sphere represent the crystal directions in (a) and are not drawn to scale. Any point on the sphere with the unit radius represents the tip of a unit vector, which is drawn from the center of the sphere (intersection of the three crystal planes). In this figure, two of the crystal planes are perpendicular and are not seen. The surface of the sphere covers all possible 3D arbitrary unit vectors.

noted that the C–S–H gel at an early stage resembles tobermorite 14 Å, while it resembles jennite after a period of months or years.[7,46] Thus, if there is any metastable structure in between and consistent with the C–S–H thermodynamic equilibrium, it may have the same average elastic properties as these two minerals.

Having the atomic coordinates for each deformation, we can compute the average directional bond strain in Ca–O, Si—O, and O–H in each of *X*, *Y*, and *Z* directions. Figure 6 shows that average directional bond strains have following common characteristics:

First, in all crystals under constant strain of 1%, Ca–O bond strains are greater than Si–O bond strains, indicating that Si–O bonds are much stronger than Ca–O bonds. Note that while the total applied strain is 1%, each individual bond strain can in general be larger than 1%. Second, for tobermorite 14 Å and jennite, O–H strains are always greater than corresponding strains in other minerals under study. This indicates a structural role of O–H bonds in these two C–S–H analogs, which have large amount of water molecules in the interlayer distance. The large values of the O–H strains in jennite and tobermorite 14 Å indicate that the water molecules act as a weak bridge in the interlayer bond connecting adjacent layers, that is Si(OH)–H_2O–Si(OH). These water molecules are part of the crystal-chemistry of the mineral and are not bulk water; that is, they are attached to the layers and cannot freely move in the interlayer space. This is analogous to the studies of state of water in Portland cement pastes.[47]

Table IV. Reuss–Voigt–Hill Average of the Elastic Constants for the Tobermorite Family and Jennite Obtained from First-Principles Calculation

	Tobermorite (Merlino)			Tobermorite (Hamid, 11 Å)			Jennite
	14 Å	11 Å	9 Å	Ca/Si = 1	Ca/Si = 0.83	Ca/Si = 0.67	Ca/Si = 1.5
K (GPa)	35.91	66.65	71.42	60.84	58	52.68	31.83
G (GPa)	20.61	32.03	37.18	35.97	32.56	29.81	21.96
M (GPa)	55.64	90.59	103.03	96.31	88.44	80.77	56.26
E (GPa)	51.90	82.82	95.06	90.14	82.29	75.23	53.55

V. Discussion and Conclusions

In the present work, using first-principles calculations we found lattice parameters and elastic constants for two classes of complex layered hydrated oxides, tobermorite family and jennite. For tobermorite 14 Å, the large interlayer distance makes the coulombic interlayer interactions relatively insignificant compared with the iono-covalent intralayer interactions. In addition, the existence of water molecules as well as Ca ions in the interlayer space shield the coulombic interlayer interactions. Thus as expected, the interlayer direction is the softest direction.

By decreasing the interlayer distance to 11 Å, the long-range coulombic interlayer interactions become comparable to the iono-covalent intralayer interactions. In this case, the softest directions are two inclined regions that form a hinge mechanism. By quantifying total coulombic energy in the interlayer direction for different isomorphs of tobermorite 11 Å (Hamid types), we showed that adding Ca in the interlayer space shields the coulombic interlayer interactions, and thus shifts the two inclined soft regions toward a single straight interlayer direction.

In summary, in contrast to the common perception that layered materials are soft in layer direction, we found that this is not the case if the interlayer distance is such that the long-range coulombic interlayer interactions are comparable to the covalent intralayer interactions. However, this is not the only require-

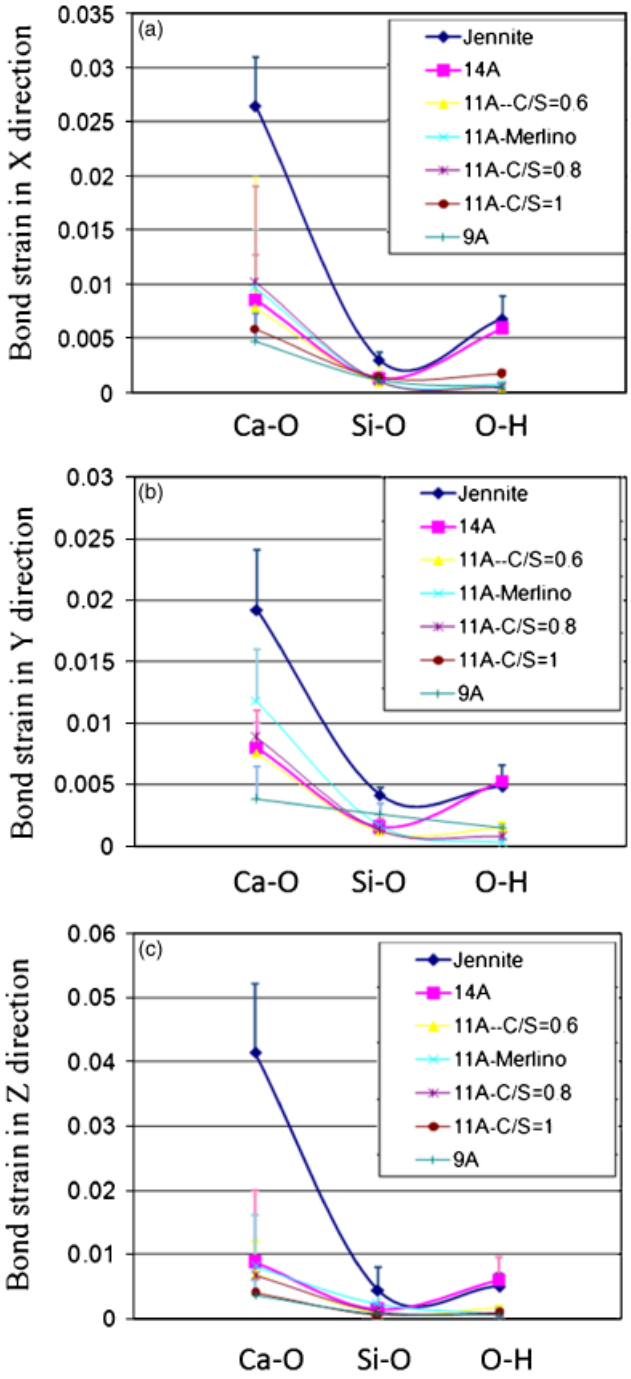

Fig. 6. Average bond strains in Ca–O, Si—O, and O–H for different C–S–H crystals. Applied strain on all crystals is 0.01: (a) average bond strains in *X* direction; (b) average bond strains in *Y* direction; (c) average bond strains in *Z* direction. In all figures the bar symbols indicate the positive error.

ment, and the existence of interlayer ions and water molecules may shield the coulombic interlayer interactions. In the case of tobermorite 11 Å (Merlino type) and tobermorite 9 Å, the covalent interlayer bonds considerably strengthen the interlayer direction, which lead to hinge (gliding) mechanism.

Finally, we characterized tobermorite family and jennite based on their average elastic properties. By monitoring bond length changes we showed that (i) Si–O bonds are much stronger than Ca–O bonds. (ii) H_2O molecules in tobermorite 14 Å and jennite—compared with other studied minerals—have a structural role and are part of a Si(OH)–H_2O–Si(OH) bridge in the interlayer distance. The investigated class of materials and the method and results reported here are of general interest for chemically complex hydrated layered oxides such as C–S–H. This opens the route to the study of elastic properties at the atomistic scale of other hydrated layered minerals such as clay minerals that are of central importance in soil sciences or Serpentines minerals involved in earth-quake mechanisms and more generally in tectonophysics.

Last, the results presented here may also serve as a benchmark for validation of empirical force fields commonly employed in atomistic investigations of core properties of complex hydrated oxides.

Acknowledgments

We are grateful to Prof. Sidney Yip (MIT) for his helpful comments and suggestions throughout the completion of this work, Prof. Nicola Marzari (MIT), and Prof. Arash Mostofi (Imperial College) for useful discussions on DFT calculations.

References

[1]H. F. W. Taylor, *Chemistry of Cement*. Academic Press, New York, 1964.
[2]A. J. Allen, J. J. Thomas, and H. M. Jennings, "Composition and Density of Nanoscale Calcium-Silicate-Hydrate in Cement," *Nat. Mater.*, **6**, 311–6 (2007).
[3]X. Zhang, W. Chang, T. Zhang, and C. K. Ong, "Nanostructure of Calcium Silicate Hydrate Gels in Cement Paste," *J. Am. Ceram. Soc.*, **83**, 2600–4 (2000).
[4]P. Colombet, A.-R. Grimmer, H. Zanni, and P. Sozzani, *Nuclear Magnetic Resonance Spectroscopy of Cement Based Materials*. Springer, Berlin, 1996.
[5]Viehland D., L. J. Yaun, Z. Xu, X. Cong, and R. J. Kirkpatrick, "Structural Studies of Jennite and 1.4 nm Tobermorite: Distorted Layering along the [100] of Jennite," *J. Am. Ceram. Soc.*, **80**, 3021–8 (1997).
[6]R. J.-M. Pellenq, N. Lequeux, and H.van Damme, "Engineering the Bonding Scheme in C–S–H: The Iono-Covalent Framework," *Cem. Concr. Res.*, **38**, 159–74 (2008).
[7]H. F. W. Taylor, "Proposed Structure for Calcium Silicate Hydrate Gel," *J. Am. Ceram. Soc.*, **69**, 464–7 (1986).
[8]I. G. Richardson and G. W. Groves, "Models for the Composition and Structure of Calcium Silicate Hydrate (C–S–H) Gel in Hardened Tricalcium Silicate Pastes," *Cem. Concr. Res.*, **22**, 1001–10 (1992).
[9]I. G. Richardson, "Tobermorite/Jennite- and Tobermorite/Calcium Hydroxide-Based Models for the Structure of C–S–H: Applicability to Hardened Pastes of Tricalcium Silicate, β-Dicalcium Silicate, Portland Cement, and Blends of Portland Cement with Blast-Furnace Slag, Metakaolin, or Silica Fume," *Cem. Concr. Res.*, **34**, 1733–77 (2004).
[10]S. Merlino, E. Bonnacorsi, and T. Armbruster, "The Real Structure of Clinotobermorite and Tobermorite 9 Å: OD Character, Polytypes, and Structural Relationships," *Eur. J. Miner.*, **12**, 411–29 (2000).
[11]S. Merlino, E. Bonnacorsi, and T. Armbruster, "The Real Structure of Tobermorite 11 Å: Normal and Anomalous Forms, OD Character and Polytyptic Modifications," *Eur. J. Miner.*, **13**, 577–90 (2001).
[12]E. Bonnacorsi and S. Merlino, "Modular Microporous Minerals: Cancrinite-Davyne Group and C–S–H Phases," *Rev. Mineral. Geochem.*, **57**, 241–90 (2005).
[13]E. Bonnacorsi, S. Merlino, and H. F. W. Taylor, "The Crystal Structure of Jennite $Ca_9Si_6O_{18}(OH)_6 \cdot 8H_2O$," *Cem. Concr. Res.*, **34**, 1481–8 (2004).
[14]E. Bonnacorsi and S. Merlino, "The Crystal Structure of Tobermorite 14 Å (Plombierite), a C–S–H Phase," *J. Am. Ceram. Soc.*, **88**, 505–12 (2005).
[15]J. D. C. McConnell, "The Hydrated Calcium Silicates Riversideite, Tobermorite, and Plombierite," *Mineral. Mag.*, **30**, 293–305 (1954).
[16]W. Wieker, A.-R. Grimmer, A. Winkler, M. Magi, M. Tarmak, and E. Lippmaa, "Solid-State High Resolution ^{29}Si NMR Spectroscopy of Synthetic 14 Å, 11 Å, and 9 Å Tobermorites," *Cem. Concr. Res.*, **12**, 333–9 (1982).
[17]S. Komarneni, D. M. Roy, C. A. Fyfe, and G. J. Kennedy, "Naturally Occurring 1.4nm Tobermorite and Synthetic Jennite: Characterization by Al and Si MASNMR Spectroscopy and Cation Exchange Properties," *Cem. Concr. Res.*, **17**, 891–5 (1987).
[18]X. Cong and R. J. Kirkpatrick, "^{29}Si and ^{17}O NMR Investigation of the Structure of Some Crystalline Calcium Silicate Hydrates," *Adv. Cem. Bas. Mat.*, **3**, 133–43 (1996).
[19]P. Yu and R. J. Kirkpatrick, "Thermal Dehydration of Tobermorite and Jennite," *Concr. Sci. Eng.*, **1**, 185–91 (1999).
[20]T. Maeshima, H. Noma, M. Sakiyama, and T. Mitsuda, "Natural 1.1 and 1.4nm Tobermorites from Fuka, Okayama, Japan: Chemical Analysis, Cell Dimensions, Si NMR and Thermal Behavior," *Cem. Concr. Res.*, **42**, 229–35 (1978).
[21]S. A. Hamid, "The Crystal Structure of the 11 Å Natural Tobermorite," *Zeitschrift fur kristallographie*, **154**, 189–98 (1981).
[22]S. V. Churakov, "Structure of the Interlay in Normal 11Å Tobermorite from Ab Initio Study," *Eur. J. Mineral*, 101127 (2009).
[23]S. A. Churakov, "Hydrogen Bond Connectivity in Jennite from Ab Initio Simulations," *Cem. Concr. Res.*, **38**, 1359–64 (2008).
[24]P. Hohenberg and W. Kohn, "Inhomogeneous Electron Gas," *Phys. Rev. B*, **136**, 71–84 (1964).
[25]W. Kohn and L. J. Sham, "Seld-Consistent Equations Including Exchange and Correlation Effects," *Phys. Rev. A*, **140**, 1133–8 (1965).
[26]D. Vanderbilt, "Self-Consistent Pseudopotentials in a Generalized Eigenvalue Formalism," *Phys. Rev. B*, **41**, 7892–5 (1990).
[27]S. Baroni, A. Dal Corso, S. de Gironcoli, and P. Giannozzi, http://www.pwscf.org

[28]H. Nielson and R. M. Martin, "First-Principle Calculations of Stress," *Phys. Rev. Lett.*, **50**, 697–700 (1983).
[29]H. Yao, L. Ouyang, and W.-Y. Ching, "*Ab initio* Calculation of Elastic Constants of Ceramic Crystals," *J. Am. Ceram. Soc.*, **90**, 3194–204 (2007).
[30]Y. Le Page and P. Saxe, "Symmetry-General Least-Sqaure Extraction of Elastic Data for Strained Materials from *ab initio* Calculations of Stress," *Phys. Rev. B*, **65**, 104104 (2002).
[31]V. R. Saunders, R. Dovesi, C. Roetti, R. Orlando, C. M. Zicovich-Wilson, N. M. Harrison, K. Doll, B. Civalleri, I. J. Bush, Ph. D'Arco, and M. Llunell, Crystal06, User's Manual, University of Torino (2006). http://www.crystal.unito.it
[32]M. Corno, C. Busco, B. Civalleri, and P. Ugliengo, "Periodic ab initio Study of Structural and Vibrational Features of Hexagonal Hydroxyapatite $Ca_{10}(PO_4)_6(OH)_2$," *Phys. Chem. Chem. Phys.*, **8**, 2464–72 (2006).
[33]W. Kohn, Y. Meir, and D. E. Makarov, "Van der Waals Energies in Density Functional Theory," *Phys. Rev. Lett.*, **80**, 4153–6 (1998).
[34]H. Rydberg, M. Dion, N. Jacobson, E. Schroder, P. Hyldgaard, S. I. Simak, D. C. Langreth, and B. I. Lundqvist, "Van der Waals Density Functional for Layered Structures," *Phys. Rev. Lett.*, **91**, 126402 (2003).
[35]Jmol: an open-source Java viewer for chemical structures in 3D. http://www.jmol.org/
[36]J. F. Nye, *Physical Properties of Crystals*. Oxford University Press, Oxford: England, 1957.
[37]H. J. Monkhorst and J. D. Pack, "Special Points for Brillouin-Zone Integrations," *Phys. Rev. B*, **13**, 5188–92 (1976).
[38]R. J.-M Pellenq and H. Van Damme, "Why Does Concrete Set: The Nature of Cohesion Forces in Hardened Cement Based Materials," *MRS Bull.*, 319–23 (2004).
[39]W. Voigt, *Lehrbuch der kristallphysik*. Taubner, Leipzig, 1928.
[40]A. Reuss and Z. Angew, "Berchung der fiessgrenze von mischkristallen auf grund der plastiziatsbedingung fur einkristalle," *Math. Mech.*, **9**, 55–8 (1929).
[41]R. Hill, "The Elastic Behavior of a Crystalline Aggregate," *Proc. Phys. Soc. Lond.*, **65**, 350–4 (1952).
[42]L. A. Galin, *Contact Problems in Theory of Elasticity*. Gostekhizdat, Moscow, 1953.
[43]I. N. Sneddon, "The Relation Between Load and Penetration in the Axisymmetric Boussinesq Problem for a Punch of Arbitrary Profile," *Int. J. Eng. Sci.*, **3**, 47–57 (1965).
[44]G. Constantinides and F.-J. Ulm, "The Nanogranular Nature of C–S–H," *J. Mech. Phys. Sol.*, **55**, 64–90 (2007).
[45]F.-J. Ulm, M. VanDamme, C. Bobko, J. A. Ortega, K. Tai, and C. Ortiz, "Statistical Indentation Techniques for Hydrated Nanocomposites: Concrete, None, and Shale," *J. Am. Ceram. Soc.*, **90**, 2677–92 (2007).
[46]J. J. Chen, J. J. Thomas, H. F. W. Taylor, and H. M. Jenning, "Solubility and Structure of Calcium Silicate Hydrate," *Cem. Concr. Res.*, **34**, 1499–519 (2004).
[47]J. J. Thomas, S. A. FitzGerlad, D. A. Nuemann, and R. A. Livingston, "State of Water in Hydrating Tricalcium Silicate and Portland Cement Pastes as Measured by Quasi-Elastic Nuetron Scaterring," *J. Am. Ceram. Soc.*, **84**, 1811–6 (2001). □